Magnetization Slow Dynamics in Ferrocenium Complexes

Mei Ding,[a] Anne K. Hickey,[a] Maren Pink,[a] Joshua Telser,*[b] David L. Tierney,[c] Martin Amoza,[d] Mathieu Rouzières,[e],[f] Tarik J. Ozumzerzifon,[g] Wesley A. Hoffert,[g] Matthew P. Shores,[g] Eliseo Ruiz,*[d] Rodolphe Clérac*[e],[f] and Jeremy M. Smith*[a]

Abstract: The Single-Molecule Magnet (SMM) properties of a series of ferrocenium complexes, $[Fe(\eta_5\text{-}C_5R_5)_2]_+$ (R = Me, Bn), are reported. In the presence of an applied dc field, the slow dynamics of the magnetization in $[Fe(\eta_5\text{-}C_5Me_5)_2]BAr_F$ are revealed. Multireference quantum mechanical calculations show a large energy difference between the ground and first excited states, excluding the commonly invoked, thermally activated (Orbach-like) mechanism of relaxation. In contrast, a detailed analysis of the relaxation time highlights that both direct and Raman processes are responsible for the SMM properties. Similarly, the bulky ferrocenium complexes, $[Fe(\eta_5\text{-}C_5Bn_5)_2]BF_4$ and $[Fe(\eta_5\text{-}C_5Bn_5)_2]PF_6$, also exhibit magnetization slow dynamics, however an additional relaxation process is clearly detected for these analogous systems.

Introduction

As the commonly accepted progenitor of organometallic chemistry, ferrocene has seen a myriad of applications since the report of its discovery in 1951.[1] The synthetic flexibility and well-defined redox properties have led to an enormous number of ferrocene-containing ligands, molecules and materials.[2-5] Amazingly, over sixty years since its discovery, fundamental discoveries regarding ferrocene and its derivatives are still being reported, as exemplified by the recent isolation of the remarkable Fe(IV) complex, $[Fe(\eta_5\text{-}C_5Me_5)_2]_{2+}$.[6]

It is notable that the canonical d-orbital manifold for metallocenes resembles that for four-coordinate complexes in three-fold symmetry (**Figure 1**),[7] where the degenerate d_{xz}, d_{yz} orbitals are strongly antibonding, d_{z2} is largely a non-bonding orbital and the degenerate d_{x2-y2}, d_{xy} are bonding orbitals. The electronic structure of this latter class of complexes can lead to remarkable magnetic properties, such as spin-crossover, Single-Molecule Magnet (SMM), or photoinduced SMM properties for example for iron(II) tris(carbene)borate complexes.[8-11] More recently, we have found that the low spin d_3 (S = ½) Mn(IV) complex $PhB(MesIm)_3Mn{\equiv}N$, which has an ^2E ground state,[12] displays slow relaxation of the magnetization, and thus can be classified as an SMM.[13] Theoretical investigations revealed that this behavior originates from an anisotropic ground doublet that is stabilized by spin–orbit coupling. In light of the analogous electronic structures (**Figure 1**), we hypothesized that metallocene complexes with the appropriate d-electron count may likewise show SMM properties.

[a] Dr. M. Ding, Dr. A.K. Hickey, Dr. M. Pink, Prof. J.M. Smith
Department of Chemistry,
Indiana University
800 E. Kirkwood Ave., Bloomington, Indiana 47401, United States.
E-mail: smith962@indiana.edu

[b] Prof. J. Telser
Department of Biological, Chemical and Physical Sciences
Roosevelt University
Chicago, Illinois 60605 United States
E-mail: jtelser@roosevelt.edu

[c] Prof. D.L. Tierney
Department of Chemistry and Biochemistry
Miami University
Oxford, Ohio 45056, United States

[d] M. Amoza, Prof. E. Ruiz
Departament de Química Inorgànica i Orgànica, Institut de Recerca de Química Teòrica i Computacional
Universitat de Barcelona
Diagonal 645, Barcelona, 08028 Spain
E-mail: jtelser@roosevelt.edu

[e] M. Rouzières, Dr. Hab. R. Clérac
CNRS, CRPP, UMR 5031, 33600 Pessac, France
E-mail: clerac@crpp-bordeaux.cnrs.fr

[f] M. Rouzières, Dr. Hab. R. Clérac
Univ. Bordeaux
CRPP, UMR 5031, 33600 Pessac, France.

[g] T.J. Ozumzerzifon, W.A. Hoffert, Prof. M.P. Shores
Department of Chemistry
Colorado State University
Fort Collins, Colorado 80523, United States.

Supporting information for this article is given via a link at the end of the document.

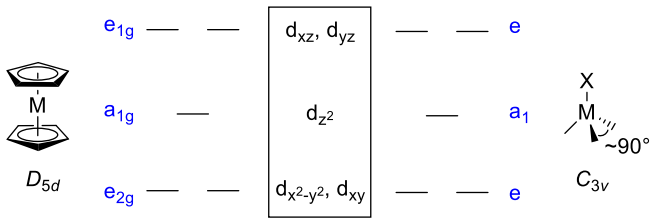

Figure 1. Canonical d-orbital manifold for metallocenes (left, in staggered geometry) and certain three-fold symmetric complexes with tripodal ligands (right). Note that lower two energy levels may have a different relative ordering.[7]

Ferrocene and its derivatives can be readily and reversibly oxidized to low spin d_5 (S = ½) ferrocenium cations, $[Fe(\eta_5\text{-}C_5R_5)_2]_+$. Magnetic susceptibility[14,15] and EPR[16,17] experiments have established the electronic ground state of ferrocenium to be $^2E_{2g}[(a_{1g})^2(e_{2g})^3]$, where the relative energies of the a_{1g} and e_{2g} levels has changed from the canonical electronic structure. The orbital degeneracy of this electronic configuration gives rise to highly anisotropic g values, which are observed in the EPR spectra of ferrocenium cations. This four-fold degenerate electronic state is split into two Kramers doublets by the combined action of the spin-orbit coupling (SOC) interaction and a low symmetry perturbation. Since this latter perturbation is only slightly larger than the SOC, it is only partially quenched. This unquenched SOC leads to magnetic moments that are significantly larger than the S = ½ spin only value.

Understanding the magnetization dynamics of a paramagnetic complex requires an accurate knowledge of the various mechanisms involved. For a paramagnetic metal complex, *four* mechanisms are generally used to describe the magnetization relaxation in the solid state, each of which has a characteristic temperature (T) and dc-field (H) dependence. The global relaxation rate (denoted τ^{-1} with τ being the relaxation time) is then usually described by a combination of all or some of these mechanisms, specifically Orbach, direct, quantum tunneling (QTM) and Raman processes, although other processes have been proposed:[18]

$$\tau^{-1} = \tau_{Orbach}^{-1} + \tau_{direct}^{-1} + \tau_{QTM}^{-1} + \tau_{Raman}^{-1}$$
$$= \tau_0^{-1}\exp\left(-\frac{\Delta}{k_BT}\right) + aTH^4 + \left(\frac{1+b_1}{1+b_2H^2}\right) + d\left(\frac{1+eH^2}{1+fH^2}\right)T^n \quad (1)$$

where Δ is the magnetic anisotropy barrier, τ_0 is an attempt time, and a, b_1, b_2, d, e, f and n are reduced parameters linked to the different relaxation pathways (see reference [18]). The last contribution, which includes the Brons-van Vleck term[19] as a prefactor, describes both the field and temperature dependence of the Raman process at low magnetic fields. In zero field, this Raman term is equivalent to the commonly used dT^n expression, e.g. in EPR spectroscopy (it is worth noting that the d parameter corresponds to the zero-field relaxation). The e parameter is highly dependent on the paramagnetic center concentration and introduces the relaxation of the interacting spins while the f parameter indicates the effect of the external field to suppress the spin relaxation. It is also interesting to mention the resemblance of the Brons-van Vleck term to the QTM term. For an S = ½ Kramers ion such as ferrocenium, which has no barrier, tunneling can contribute to the spin relaxation just by the transition between two states with opposite spin.

The spin-lattice relaxation dynamics of ferrocenium ions have been investigated spectroscopically. At temperatures above 80 K, the spin-lattice relaxation dynamics of ferrocenium-containing materials was proposed to follow an Orbach-like mechanism, as determined by ^{57}Fe Mössbauer spectroscopy.[20-24] However, the solid state relaxation dynamics of some very bulky ferrocenium salts do not follow a simple Orbach-like mechanism at lower temperatures.[20-23] At very low temperatures, the relaxation of some bulky ferrocenium complexes is observed to be slow on the Mössbauer timescale, as evidenced by the appearance of hyperfine interactions in the spectrum,[20-23] which was first observed for $[Fe(\eta_5\text{-}(1,3\text{-}Me_3Si)_2C_5H_3)_2]OTf$.[25]

In this paper, we report a detailed analysis of the magnetization dynamics in some ferrocenium-based materials. To reduce the possible effects of dipolar magnetic interactions on the magnetization dynamics, we chose to investigate ferroceniums having bulky cyclopentadienyl ring substituents and/or large counterions, allowing the magnetic centers to be well-separated in the solid state. Specifically, the bulky cyclopentadienyl ligands in $[Fe(\eta_5\text{-}C_5Bn_5)_2]X$ (X = BF_4- and PF_6-)[26] and the large counterion in $[Fe(\eta_5\text{-}C_5Me_5)_2]BAr^F$[27] are expected to provide long Fe...Fe separations in the solid state (**Scheme 1**).

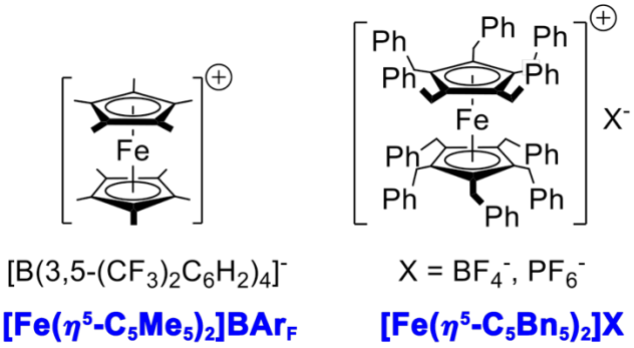

Scheme 1. Ferrocenium complexes investigated in this work.

Results and Discussion

Synthesis, Structural and Spectroscopic Characterization

The bulky ferrocene, $Fe(\eta_5\text{-}C_5Bn_5)_2$, was prepared from pentabenzylcyclopentadienyl lithium and anhydrous $FeCl_2$, similarly to literature procedures.[28,29] As previously reported, oxidation to the ferrocenium complexes, $[Fe(\eta_5\text{-}C_5Bn_5)_2]BF_4$ and $[Fe(\eta_5\text{-}C_5Bn_5)_2]PF_6$, was accomplished using $NOBF_4$ and $AgPF_6$ oxidants, respectively.[25] The molecular structure of $[Fe(\eta_5\text{-}C_5Bn_5)_2]BF_4$ was determined by single-crystal X-ray diffraction, revealing the anticipated ferrocenium complex (**Figure 2**) that crystallizes along with interstitial CH_2Cl_2 molecules. As previously observed,[25] the cyclopentadienyl rings are staggered, with Fe-C (2.100(4) – 2.114(4) Å) and cyclopentadienyl C-C distances 1.427(7) – 1.446(6) Å that are typical for ferrocenium complexes.[30] The angle between the cyclopentadienyl rings is 0.47°. Importantly and as expected, the paramagnetic iron centers are well-separated in the solid state, with the nearest Fe...Fe distance being 11.208(1) Å.

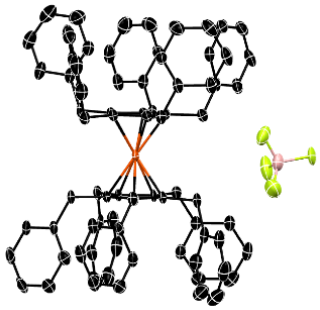

Figure 2. X-ray crystal structure of $[Fe(\eta_5\text{-}C_5Bn_5)_2]BF_4$. Thermal ellipsoids shown at 50% probability, hydrogen atoms and cocrystallized CH_2Cl_2 solvent omitted for clarity. Black, orange, pink and lime ellipsoids represent C, Fe, B and F atoms, respectively.

Unfortunately, while we were able to determine the connectivity for the cation in $[Fe(\eta_5\text{-}C_5Bn_5)_2]PF_6$, the diffraction data were too weak to obtain any meaningful metrical information. On the other hand, the structure of $[Fe(\eta_5\text{-}C_5Me_5)_2]BAr_F$ was previously reported.[26] The iron atoms are also well-separated in this structure, with the nearest Fe...Fe distance being 9.6116 Å. The angle between cyclopentadienyl rings is 2.72°, suggesting a slightly lower local symmetry than for $[Fe(\eta_5\text{-}C_5Bn_5)_2]BF_4$. These three complexes were characterized by low temperature EPR spectroscopy, while $[Fe(\eta_5\text{-}C_5Bn_5)_2]BF_4$ was also characterized by variable temperature ^{57}Fe Mössbauer spectroscopy (**Figures S3 and S4**). On decreasing the temperature, the single absorption signal in the spectrum at 80 K (δ = 0.57 mm/s) resolves into six lines at 4.5 K, indicative of slow relaxation of the magnetization on the timescale of the Mössbauer experiment. Similar behavior has been reported for other bulky ferrocenium complexes.[20-23]

Magnetic Properties

The magnetic properties of the ferrocenium complexes have been studied by dc and ac techniques (see Supporting Information). Since the dc magnetic data could not be fit to a simple model, they were simulated using the results of the theoretical calculations (see below). As illustrated for $[Fe(\eta_5\text{-}C_5Me_5)_2]BAr_F$, the χT product at 270 K has a value of 1.06

cm3 K mol−1, in agreement with a magnetically isolated low-spin (S = ½) Fe(III) center with substantial spin-orbit coupling (**Figure 3**). The large deviation from the spin-only value has been previously noted.[14,15,20-23,31] As the temperature is lowered, the χT product decreases linearly, followed by a downturn around 60 K to reach 0.79 cm3 K mol−1 at 1.85 K. The field dependences of the magnetization below 8 K for [Fe(η5-C5Me5)2]BArF are in good agreement with an S = ½ species with a magnetization that reaches 1.33 μB at 7 T & 1.85 K (**Figure 3 inset**). These experimental M versus H data can be fitted qualitatively well to an S = ½ Brillouin function providing an average g factor around 2.65(5). Similar results, shown in the Supporting Information, are observed for the other ferrocenium complexes [Fe(η5-C5Bn5)2]BF4 (g = 2.33(5)) and [Fe(η5-C5Bn5)2]PF6 (g = 2.40(5)).

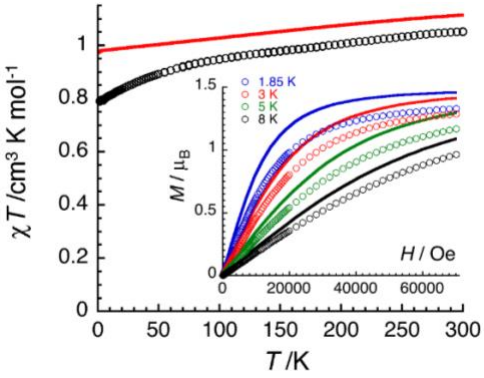

Figure 3. Temperature dependence of the χT product at 0.1 T for [Fe(η5-C5Me5)2]BArF (χ is defined as magnetic susceptibility equal to M/H per mole of [Fe(η5-C5Me5)2]BArF). Inset: field dependence of the magnetization below 8 K for [Fe(η5-C5Me5)2]BArF (8–280 mT min-1). Solid lines are simulations using the NEVPT2 results discussed in the text (see Electronic Structure Calculations section).

The magnetization dynamics of the three ferrocenium complexes have been probed by ac susceptibility measurements. In the absence of a dc field and above 1.8 K, no significant out-of-phase component of the ac susceptibility for frequencies up to 10 kHz was observed for any of the complexes. However, application of a dc field leads to the appearance of frequency dependent signals in both components of the ac susceptibility, revealing the slow dynamics of the magnetization. As shown for [Fe(η5-C5Me5)2]BArF (**Figure 4**), a maximum in the out-of-phase component becomes detectable for an applied dc field of 100 Oe. At all fields, the χ' versus ν and χ'' versus ν data can be fit to a generalized Debye model (**Figure 4**) with a small α coefficient (< 0.4; **Figure S8**) indicating a narrow distribution of the relaxation time (τ).

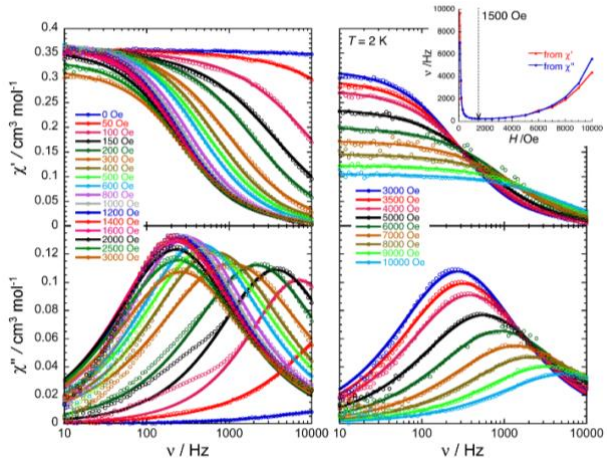

Figure 4. Frequency dependence of the real (χ', top) and imaginary (χ'', bottom) components of the ac susceptibility at 2 K at different dc fields between 0 and 1 T for a polycrystalline sample of [Fe(η5-C5Me5)2]BArF. Solid lines are the best fits of the experimental data to the generalized Debye model (see Supporting Information). Inset: Field dependence of the characteristic ac frequency (ν) deduced from the generalized Debye model fits of the χ' vs. ν (red dots) and χ'' vs. ν (blue dots) data. The solid lines are guides for the eyes.

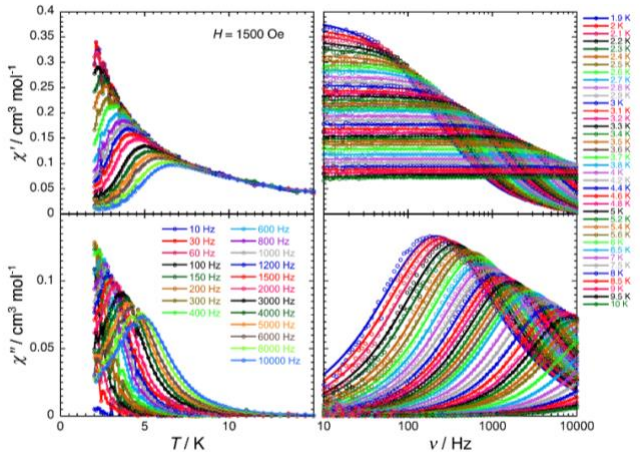

Figure 5. Temperature (left) and frequency (right) dependences of the real (χ', top) and imaginary (χ'', bottom) components of the ac susceptibility, between 1.9 and 15 K and between 10 and 10000 Hz respectively, for [Fe(η5-C5Me5)2]BArF in a 1500-Oe dc field. Solid lines are visual guides on the left part of the figure; they are the best fits of the experimental data to the generalized Debye model (see Supporting Information) on the right part of the figure.

The field dependence of the characteristic relaxation frequency at 2 K reveals that relaxation time, τ, is maximum for an optimum applied dc field of 1500 Oe (**Figure 4 inset** and **Figure S8**). Variable–frequency and –temperature ac susceptibility data for this complex were thus collected under 1500 Oe between 1.9 and 15 K (**Figure 5** and **Figure S9**) to determine the temperature dependence of the relaxation time. The observed curvature of the resulting τ versus T^{-1} plot (at 1500 Oe) in **Figure 6** suggests the presence of competing relaxation processes. A rapid analysis of the temperature dependence of the relaxation time (**Figure 6**) could conclude (i) at an exponential behavior (thermally activated) above 4 K suggesting an Orbach-like mechanism[32] of relaxation (first term of equation 1: $\tau_0 = 5.7(5) \times 10^{-7}$ s; $\Delta/k_B = 17.6(5)$ K (12.2 cm^{-1})) and (ii) below 4 K to the effect of the quantum tunneling of the relaxation (second term of equation 1). But as shown by the electronic structure calculations (*vide infra*), an Orbach-like relaxation mechanism is not relevant in the present Kramers systems. Similar ac susceptibility measurements for [Fe(η5-C5Bn5)2]BF4 and [Fe(η5-C5Bn5)2]PF6 (see Supporting Information; **Figures S10-S17**) also reveal that the relaxation time is strongly both dc-field and temperature dependent.

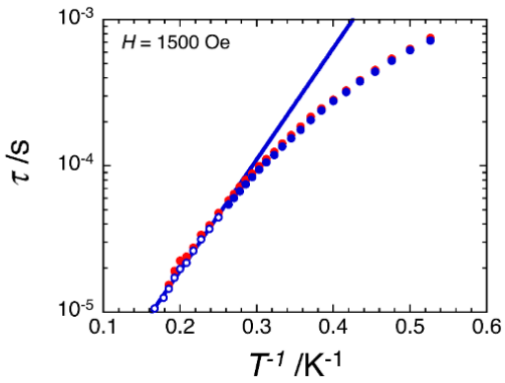

Figure 6. Temperature dependence of the relaxation time (τ) shown in semilogarithm τ vs. T^{-1} plot (Arrhenius plot) for [Fe(η5-C5Me5)2]BArF constructed from the generalized Debye fits of the χ' vs. ν (red dots) and χ'' vs. ν (blue dots) obtained under a dc field of 1500 Oe.

Electronic Structure Calculations

At first glance, the canonical metallocene electronic structure as in **Figure 1** is not consistent with the relatively large easy-axis character found experimentally, for example by EPR (**Figure S5**). The suggested electronic $e_{2g}^4 a_{1g}^1$ configuration leads to first excitation energies between $d_{x^2-y^2}/d_{xy}$ ($m_l = \pm 2$) and d_{z^2} ($m_l = 0$) that cannot provide significant spin-orbit contributions (due to the +2 difference of $|m_l|$ values for the orbitals involved in such excitations). In order to explain this discrepancy, we performed spin-orbit CASSCF calculations on the crystal structure of the [Fe(η5-C5Me5)2]+

molecule (Orca 4.0 code[39,40] with a def2-TZVP basis set[41,42]). The use of a relatively large active space of 10 orbitals with 9 electrons to include the five Fe 3d orbitals, the two occupied M-L bonding ligand orbitals and three empty orbitals provides an S = ½ ground state in agreement with the experimental data. A smaller active space considering only the five orbitals results in an incorrect (S = 5/2) ground state (note that manganocene, $[Mn(\eta_5\text{-}C_5H_5)_2]$, does have this high spin ground state[43]). This problem can also be solved for the smaller active space by adding dynamic correlation, for instance with the NEVPT2 approach.[44] The results for the $[Fe(\eta_5\text{-}C_5Bn_5)_2]_+$ complex (see Supporting Information) are qualitatively similar to those of the $[Fe(\eta_5\text{-}C_5Me_5)_2]_+$ system, thus, we will focus the discussion in the main text in this latter system. The presented results correspond to the NEVPT2 calculations including spin-orbit effect (quasi-degenerate perturbation theory, QDPT) using the 5-orbitals active space by calculating all 75 doublet, 24 quadruplet and one sextet state (to give a total of 252 microstates). The 5-orbital active space was finally selected because it allows to perform an Ab Initio ligand field (AILFT) calculation after the NEVPT2/QDPT. This approach gives a high-quality d orbital energy splitting that helps to describe the magnetic anisotropy of the system (see **Figure 8**). The local magnetic anisotropy of this S = ½ system is illustrated in the calculated **g**-tensor with g_z = 5.42 and $g_x = g_y$ = 0.99 (g_{ave} = 2.47) eigenvalues indicating the relatively large uniaxial magnetic anisotropy (see **Figure 7** showing that g_z is almost perpendicular to the (η_5-C_5Me_5) planes).

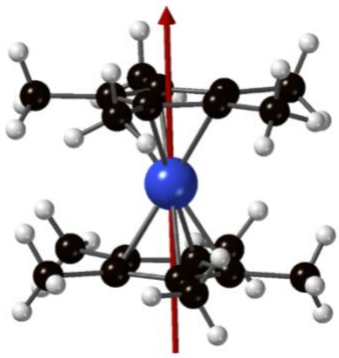

Figure 7. Representation of the NEVPT2 calculated g_z component of the **g**-tensor for $[Fe(\eta_5\text{-}C_5Me_5)_2]_+$. The z eigen-direction of the **g**-tensor is almost perpendicular to the (η_5-C_5Me_5) planes (i.e., aligned with the C_5 axis).

The simulation of the experimental data in **Figure 3** gives slightly overestimated values in the case of both M vs H and χT vs T. At 1.85 K, the magnetization reaches experimentally an almost saturation value of 1.33 μ_B at 7 T while the simulation leads to a value closer to 1.5 μ_B. Likewise, in the case of the magnetic susceptibility, the simulated χT product has a minimum of 0.97 cm^3K/mol at 1 K and a maximum at 300 K of 1.11 cm^3K/mol, compared to the respective experimental values of 0.80 and 1.05 cm^3K/mol. Importantly, the analysis of the calculated NEVPT2 ground state reveals the participation of two determinants that correspond mainly to the $e_{2g}^3a_{1g}^2$ electron configuration (weighted values of 0.70 and 0.24). These two determinants correspond to $(d_{x^2-y^2})^2(d_{xy})^1(d_{z^2})^2$ and $(d_{x^2-y^2})^1(d_{xy})^2(d_{z^2})^2$ configurations, respectively.

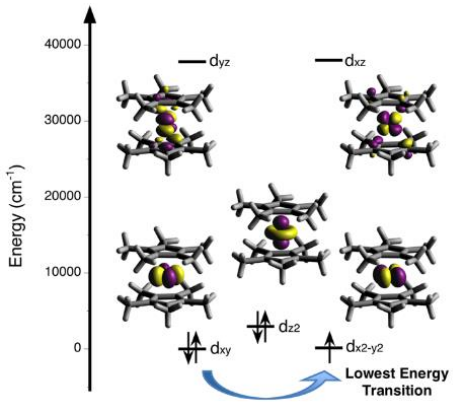

Figure 8. Energy splitting of the iron d orbitals calculated at NEVPT2 level using the AILFT (*ab initio* ligand field theory) approach.

Furthermore, the first excited state (959 cm^{-1} above the ground state, equivalent to 1380 K) has the same composition as the ground state but with an inversion of their two weighted coefficient values. Thus, the first excitation energies correspond to transitions between the $d_{x^2-y^2}$ and d_{xy} orbitals which possess the same $|m_l|$ number (see **Figure 8**) and consequently supports the presence of a large uniaxial anisotropy found experimentally in the $[Fe(\eta_5\text{-}C_5Me_5)_2]_+$ system and analogous complexes.[45,46] This anomalous occupancy of the d orbitals, i.e. filled a_{1g} (d_{z^2}) orbital at slightly higher in energy than the partially filled e_{2g} (d_{xy}, $d_{x^2-y^2}$) orbitals, indicates a smaller electronic repulsion (lesser pairing energy) in the former orbital. Finally, it is worth noting that the $[Fe(\eta_5\text{-}C_5Bn_5)_2]_+$ system (see Table SZ) is less distorted than the $[Fe(\eta_5\text{-}C_5Me_5)_2]_+$ one. The first excitation is related to the Jahn-Teller splitting of the $^2E_{2g}$ state, thus, the value for $[Fe(\eta_5\text{-}C_5Bn_5)_2]_+$ is smaller (841 cm^{-1}) and consequently, it should have larger axial character (see *g* components in Table SY).

Origin of the Magnetization Relaxation

Based on the above electronic structure calculations and the estimated position of its first excited state above 1000 K in energy, Orbach-like processes with an energy barrier as small as 17.6(5) K (as suggested by the temperature dependence of the spin relaxation time shown in **Figure 6**) can be unambiguously eliminated as being responsible for the slow dynamics of the magnetization in $[Fe(\eta_5\text{-}C_5Me_5)_2]BAr_F$. Moreover, an Orbach-like mechanism should not be considered for this system as it possesses an isolated $S = 1/2$ Kramers' doublet ground state, i.e. a two-level scheme, for which an energy barrier cannot be defined. On the other hand, quantum tunneling contribution is kept in the analysis as spin-spin dipolar interactions might be relevant in these compounds.[47] Thus, **Equation 1** may be simplified to only three terms as shown in **Equation 2**.

$$\tau^{-1} = \tau_{direct}^{-1} + \tau_{QTM}^{-1} + \tau_{Raman}^{-1} = aTH^4 + \left(\frac{1+b_1}{1+b_2H^2}\right) + d\left(\frac{1+eH^2}{1+fH^2}\right)T^n \quad (2)$$

In order to minimize the possible effects of overparametrization in the fitting procedure, the field dependence of the relaxation time at 2 K was first independently fitted to **Equation 2**. As shown in **Figure 9** (left part), **Equation 2** is able to reproduce very well the experimental data for $[Fe(\eta_5\text{-}C_5Me_5)_2]BAr_F$ by considering only direct and Raman terms with a = 2.0(2) 10^4 $K^{-1}T^{-4}s^{-1}$, e = 280(20) T^{-2}, f = 8.1(1) 10^5 T^{-2}, $2nd$ = 3.8(1) 10^6 s^{-1}. Notably, tunneling and field-dependent Raman terms are relatively similar and can both fit the low-field region. However, only the Raman term with the obtained values from the field dependence of the relaxation time can reproduce the temperature dependence (*vide infra*). Thus, at low fields (typically below 0.15 T), a Raman process induces an increase in the relaxation time, while the decrease at higher fields is attributed to the increasing importance of the direct process in applied dc field. The temperature dependence of the relaxation time at 0.15 T was analyzed analogously according to **Equation 2** (without the QTM term) fixing the a, d, e and f parameters to the values deduced from the field dependence of τ at 2 K. Therefore, the experimental τ vs T data (**Figure 9**, right part) were fitted but with only n as an adjustable parameter. Remarkably, this simple approach reproduces extremely well the experimental data with the exponent (n) of 3.8(1) for the Raman term, suggesting that relaxation involves both optical and acoustic phonons.[48] It is worth mentioning that while Kramers ions are expected to have n = 9,[32] smaller n values have been observed in a number of S = ½ transition metal complexes which display slow relaxation of the magnetization.[13,49-55]

Overall, the analysis of both field and temperature dependences of the relaxation time below 6 K and 1 T confirms that direct and Raman mechanisms are mainly responsible for the relaxation of the magnetization in $[Fe(\eta_5\text{-}C_5Me_5)_2]BAr_F$. However, since the addition of other processes in our analysis will lead to overparametrization, the presence of other active relaxation pathways cannot be totally excluded.

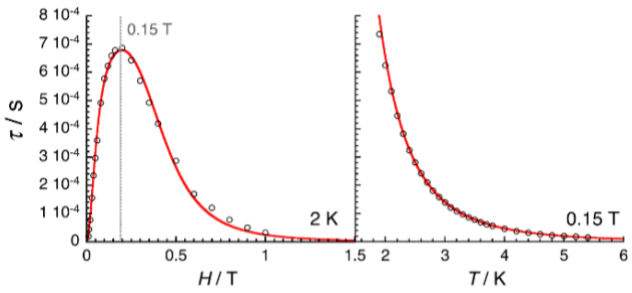

Figure 9. Field (left, at 2 K) and temperature (right, at 0.15 T) dependences of the average relaxation time for $[Fe(\eta_5\text{-}C_5Me_5)_2]BAr_F$ estimated from **Figures 4 and 5**. The red lines are the best fits obtained with the theoretical approach developed in the text using **Equation 2** (without the QTM term).

Interestingly, the observed magnetization dynamics in $[Fe(\eta_5\text{-}C_5Bn_5)_2]BF_4$ and $[Fe(\eta_5\text{-}C_5Bn_5)_2]PF_6$ differs from that of $[Fe(\eta_5\text{-}C_5Me_5)_2]BAr_F$. While a unique maximum in the field dependence of the relaxation time is seen for $[Fe(\eta_5\text{-}C_5Me_5)_2]BAr_F$ at around 0.15 T (**Figure 9**), a similar maximum is observed at 0.015 T, with a shoulder around 0.3 T for both $[Fe(\eta_5\text{-}C_5Bn_5)_2]_+$ salts (**Figures 10** and **S18** for $[Fe(\eta_5\text{-}C_5Bn_5)_2]BF_4$ and $[Fe(\eta_5\text{-}C_5Bn_5)_2]PF_6$ respectively), suggesting the presence of an additional relaxation process. While we were unable to fit the experimental τ vs H data from 0 to 1 T to only Raman and direct processes as for $Fe(\eta_5\text{-}C_5Me_5)_2]BAr_F$, it is mandatory for these two salts to include the tunneling term to fit the more complex low-field region below 0.3 T (**Equation 2**). Despite the similar field dependence of QTM and field-dependent Raman terms, it is reasonable to assume that the effect of the tunneling appears at lower fields than the Raman mechanism (as assumed in **Figure 10** for $[Fe(\eta_5\text{-}C_5Bn_5)_2]BF_4$). Thus, under the presence of a small external field, the degeneracy is lifted and consequently, the probability of relaxation through the QTM pathway is reduced. The obtained parameters are then a = 1.3(2) 10^4 $K^{-1}T^{-4}s^{-1}$, b_1=2.1(2) 10^3 s^{-1}, b_2=4.4(9) 10^4 T^{-2}, e = 1.9(5) 10^3 T^{-2}, f = 4.5(5) 10^2 T^{-2}, 1.85^nd = 252(20) s^{-1} (**Figure 10**), and a =4.2(7) 10^3 $K^{-1}T^{-4}s^{-1}$, b_1=8.4(9) 10^2 s^{-1}, b_2=72(5) 10^3 T^{-2}, e = 4.2(5) 10^2 T^{-2}, f = 2.6(5) 10^2 T^{-2}, 4^nd = 6.1(4) 10^2 s^{-1} (**Figure S18**), for $Fe(\eta_5\text{-}C_5Bn_5)_2]BF_4$ and $[Fe(\eta_5\text{-}C_5Bn_5)_2]PF_6$ respectively. Similarly to the case of $[Fe(\eta_5\text{-}C_5Me_5)_2]BAr_F$, these parameters can be used to fit the temperature dependence with only n as an adjustable parameter (n = 2.6(1) and 3.7(1)), however it is clear that the overall fits are of lower quality, which potentially supports the presence of an additional relaxation mechanisms.

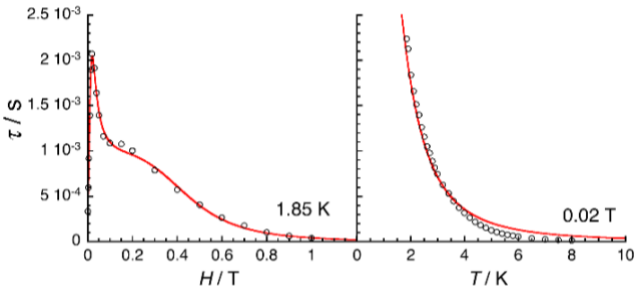

Figure 10. Field (left, at 1.85 K) and temperature (right, at 0.02 T) dependences of the average relaxation time for $[Fe(\eta_5\text{-}C_5Bn_5)_2]BF_4$ estimated from **Figures S10 and S12**. The red lines are the best fits obtained with the theoretical approach developed in the text.

Conclusions

We have shown that a series of bulky ferrocenium ions display slow relaxation of the magnetization, i.e. Single-Molecule Magnet properties, with a characteristic relaxation time that is strongly dc-field and temperature dependent. In the case of $[Fe(\eta_5\text{-}C_5Me_5)_2]BAr_F$, multireference quantum mechanical computations reveal an energy gap of over 1000 K between the ground and first excited states, excluding an Orbach-like mechanism as being the origin of the observed SMM properties. A detailed analysis of the field and temperature dependence of the relaxation time supports the theoretical calculations, revealing that both direct and Raman processes are responsible for the slow dynamics of the magnetization. In the case of $[Fe(\eta_5\text{-}C_5Bn_5)_2]BF_4$ and $[Fe(\eta_5\text{-}C_5Bn_5)_2]PF_6$, a similar analysis reveals the presence of an additional relaxation mechanism detectable at low magnetic fields, which has been attributed to quantum tunneling. The analysis of the electronic structure of the $[Fe(\eta_5\text{-}C_5Me_5)_2]_+$ system indicates a complex multireferential character in the ground state. The orbital energy splitting assuming a simple, monodeterminant approach indicates that the d_{z2} orbital should be the SOMO bearing the unpaired electron, but such electronic configuration $[(e_{2g})_4(a_{1g})_1]$ is not in agreement with the experimental magnetic properties. By contrast, NEVPT2 calculations including spin-orbit coupling effects reveal that, due to the different electronic repulsion of the orbitals, the ground state and first excited states correspond to the single-occupancy of the $d_{x2\text{-}y2}/d_{xy}$ orbitals, respectively while the d_{z2} orbital is doubly-occupied in both states. These unexpected electronic configurations of the ground and first excited states $[(a_{1g})_2(e_{2g})_3]$ are in agreement with the relatively large magnetic anisotropy found experimentally.

Our experimental results demonstrate the critical importance of analyzing the field and temperature dependence of the relaxation time. Although a naïve analysis of the temperature dependence of relaxation for these ferrocenium complexes suggests the presence of Orbach-like and quantum tunneling pathways, the field dependence shows that the relaxation is indeed dominated by a combination of direct and Raman processes. The multiple relaxation pathways that are available

to paramagnetic compounds make such analyses critical for understanding magnetization dynamics, e.g. diagnosing SMM behavior.

Acknowledgements

M.D., A.K.H. and J.M.S. acknowledge funding from Indiana University and the NSF (CHE-1112299). R.C. and M.R. thank the University of Bordeaux, the Conseil Regional de Nouvelle Aquitaine, the CNRS, the GdR MCM-2 and the MOLSPIN COST action CA15128 for financial support. T.J.O., W.A.H., and M.P.S. thank the National Science Foundation (CHE-1363274) for support. M.A and E.R. thank Spanish *Ministerio de Economía y Competitividad* (MINECO) for the grant CTQ2015-64579-C3-1-P and the computer resources, technical expertise and assistance provided by the CSUC. E.R. acknowledges Generalitat de Catalunya for an ICREA Academia award. M. A. thanks the Spanish (MINECO) for graduate FPU fellowship. We thank Prof. Brian M. Hoffman, Northwestern University, for use of the low temperature X- and Q-band EPR spectrometers, which is supported by the NIH (GM 111097 to B.M.H.).

Keywords: metallocences • magnetic properties • electronic structure • ab initio calculations

[1] T. J. Kealy and P. L. Pauson, *Nature*, **1951**, *168*, 1039-1040.
[2] I. R. Butler and D. Thomas, in *Comprehensive Organometallic Chemistry III*, Elsevier, **2007**, pp. 185-220.
[3] *Chiral Ferrocenes in Asymmetric Catalysis: Synthesis and Applications*, (Eds.: L.-X. Dai and X.-L. Hou), Wiley-VCH, Weinheim, **2010**.
[4] *Ferrocenes: Ligands, Materials and Biomolecules*, (Ed.: P. Štěpnička) John Wiley & Sons., New York, **2008**.
[5] *Ferrocenes: Compounds, Properties and Applications*, (Ed: E. S. Philips), Nova Science Publishers, New York, **2011**.
[6] M. Malischewski, K. Seppelt, M. Adelhardt, J. Sutter and K. Meyer, *Science*, **2016**, *353*, 678-682.
[7] For both classes of complex, the energy separation of between the a_{1g} (a_1) and lower lying e_{2g} (e) levels is small and may have a different relative energy ordering, depending on the metal and oxidation state. For metallocenes, see for example, T.A. Jackson, J. Krzystek, A. Ozarowski, G.B. Wijeratne, B.F. Wicker, D.J. Mindiola and J. Telser, *Organometallics* **2012**, *31*, 8265-8274 and T.A. Jackson, J. Krzystek, A. Ozarowski, G.B. Wijeratne, B.F. Wicker, D.J. Mindiola and J. Telser, *Organometallics* **2014**, *33*, 1325-1325 (addendum). For pseudotetrahedral complexes, see for example, L. Bucinsky, M. Breza, W.-T. Lee, A.K. Hickey, D.A. Dickie, I. Nieto, J.A. DeGayner, T.D. Harris, K. Meyer, J. Krzystek, A. Ozarowski, J. Nehrkorn, A. Schnegg, J. Holldack, R.H. Heber, J. Telser, and J.M. Smith, *Inorg. Chem.* **2017**, *56*, 4751-4768.
[8] M. Ding, M. Rouzières, Y. Losovyj, M. Pink, R. Clérac and J. M. Smith, *Inorg. Chem.*, **2015**, *54*, 9075-9080.
[9] H.-J. Lin, D. Siretanu, D. A. Dickie, D. Subedi, J. J. Scepaniak, D. Mitcov, R. Clérac and J. M. Smith, *J. Am. Chem. Soc.*, **2014**, *136*, 13326-13332.
[10] C. Mathonière, H.-J. Lin, D. Siretanu, R. Clérac and J. M. Smith, *J. Am. Chem. Soc.*, **2013**, *135*, 19083-19086.
[11] J. J. Scepaniak, T. D. Harris, C. S. Vogel, J. r. Sutter, K. Meyer and J. M. Smith, *J. Am. Chem. Soc.*, **2011**, *133*, 3824-3827.
[12] G. E. Cutsail III, B. W. Stein, D. Subedi, J. M. Smith, M. L. Kirk and B. M. Hoffman, *J. Am. Chem. Soc.*, **2014**, *136*, 12323-12336.
[13] M. Ding, G. E. Cutsail III, D. Aravena, M. Amoza, M. Rouzières, P. Dechambenoit, Y. Losovyj, M. Pink, E. Ruiz, R. Clérac and J. M. Smith, *Chem. Sci.*, **2016**, *7*, 6132-6140.
[14] D. N. Hendrickson, Y. S. Sohn and H. B. Gray, *Inorg. Chem.*, **1971**, *10*, 1559-1563.
[15] Y. S. Sohn, D. N. Hendrickson and H. B. Gray, *J. Am. Chem. Soc.*, **1970**, *92*, 3233-3234.
[16] R. Prins, *Mol. Phys.*, **1970**, *19*, 603-620.
[17] R. Prins and F. J. Reinders, *J. Am. Chem. Soc.*, **1969**, *91*, 4929-4931.
[18] K. N. Shrivastava, *Phys. Stat. Sol. A*, **1983**, *117*, 437-458.
[19] J. H. Van Vleck, *Phys. Rev.*, **1940**, *57*, 426-447.
[20] M. Abraham, H. H. Klauß, W. Wagener, F. J. Litterst, A. Hofmann and M. Herberhold, *Hyperfine Interact.*, **1999**, *120/121*, 253-256.
[21] R. H. Herber, I. Felner and I. Nowik, *Hyperfine Interact.*, **2016**, *237*, 100.
[22] I. Nowik and R. H. Herber, *Inorg. Chim. Acta*, **2000**, *310*, 191-195.
[23] H. Schottenberger, K. Wurst, U. J. Griesser, R. K. R. Jetti, G. Laus, R. H. Herber and I. Nowik, *J. Am. Chem. Soc.*, **2005**, *127*, 6795-6801.
[24] M. Reiners, D. Baabe, P. Schweyen, M. Freytag, P. G. Jones and M. D. Walter, *Eur. J. Inorg. Chem.*, **2017**, 388-400.
[25] A. Houlton, R. A. Brown, J. R. Miller, R. M. G. Roberts, J. Silver and M. Thomas, *J. Organomet. Chem.*, **1992**, *431*, C17-C20.
[26] P. Zanello, A. Cinquantini, S. Mangani, G. Opromolla, L. Pardi, C. Janiak and M. D. Rausch, *J. Organomet. Chem.*, **1994**, *471*, 171-177.
[27] I. Chávez, A. Alvarez-Carena, E. Molins, A. Roig, W. Maniukiewicz, A. Arancibia, V. Arancibia, H. Brand and J. Manuel Manríquez, *J. Organomet. Chem.*, **2000**, *601*, 126-132.
[28] J. W. Chambers, A. J. Baskar, S. G. Bott, J. L. Atwood and M. D. Rausch, *Organometallics*, **1986**, *5*, 1635-1641.
[29] H. Schumann, C. Janiak, R. D. Köhn, J. Loebel and A. Dietrich, *J. Organomet. Chem.*, **1989**, *365*, 137-150.
[30] C. R. Groom, I. J. Bruno, M. P. Lightfoot and S. C. Ward, *Acta Cryst.*, **2016**, *B72*, 171-179.
[31] K. D. Warren, *Inorg. Chem.*, **1974**, *13*, 1317-1324.
[32] A. Abragam and B. Bleaney, *Electron Paramagnetic Resonance of Transition Ions*, Dover, New York, **1986**.
[33] F. Aquilante, L. De Vico, N. Ferré, G. Ghigo, P.-Å. Malmqvist, P. Neogrády, T. B. Pedersen, M. Pitonak, M. Reiher, B. O. Roos, L. Serrano-Andrés, M. Urban, V. Veryazov and R. Lindh, *J. Comput. Chem.*, **2010**, *31*, 224-247.
[34] G. Karlström, R. Lindh, P.-Å. Malmqvist, B. O. Roos, U. Ryde, V. Veryazov, P.-O. Widmark, M. Cossi, B. Schimmelpfennig, P. Neograd y and L. Seijo, *Comput. Mater. Sci.*, **2003**, *28*, 222-239.
[35] V. Veryazov, P.-O. Widmark, L. Serrano-Andrés, R. Lindh and B. O. Roos, *Int. J. Quantum Chem.*, **2004**, *100*, 626-635.

[36] B. O. Roos, R. Lindh, P.-A. Malmqvist, V. Veryazov and P.-O. Widmark, *J. Phys. Chem. A.*, **2004**, *108*, 2851-2858.
[37] B. O. Roos, R. Lindh, P.-Å. Malmqvist, V. Veryazov, P.-O. Widmark and A. C. Borin, *J. Phys. Chem. A.*, **2008**, *112*, 11431-11435.
[38] P.-O. Widmark, P.-Å. Malmqvist and B. O. Roos, *Theor. Chim. Acta*, **1990**, *77*, 291-306.
[39] F. Neese, *Wiley Interdiscip. Rev. Comput. Mol. Sci.*, **2012**, *2*, 73-78.
[40] F. Neese, *Wiley Interdiscip. Rev. Comput. Mol. Sci.*, **2018**, e1327.
[41] A. Schäfer, H. Horn and R. Ahlrichs, *J. Chem. Phys.*, **1992**, *97*, 2571-2577.
[42] F. Weigend and R. Ahlrichs, *Phys. Chem. Chem. Phys.*, **2005**, *7*, 3297.
[43] M. E. Switzer, R. Wang, M. F. Rettig and A. H. Maki, *J. Am. Chem. Soc.*, **1974**, *96*, 7669-7674.
[44] C. Angeli, R. Cimiraglia, S. Evangelisti, T. Leininger and J. P. Malrieu, *J. Chem. Phys.*, **2001**, *114*, 10252-10264.
[45] S. Gómez-Coca, D. Aravena, R. Morales and E. Ruiz, *Coord. Chem. Rev.*, **2015**, *289-290*, 379-392.
[46] S. Gomez-Coca, E. Cremades, N. Aliaga-Alcalde and E. Ruiz, *J. Am. Chem. Soc.*, **2013**, *135*, 7010-7018.
[47] D. Aravena, *J. Phys. Chem. Lett.*, **2018**, *9*, 5327-5333.
[48] A. Singh and K. N. Shrivastava, *Phys. Stat. Sol. B.*, **1979**, *95*, 273-277.
[49] M. Atzori, E. Morra, L. Tesi, A. Albino, M. Chiesa, L. Sorace and R. Sessoli, *J. Am. Chem. Soc.*, **2016**, *138*, 11234-11244.
[50] M. Atzori, L. Tesi, S. Benci, A. Lunghi, R. Righini, A. Taschin, R. Torre, L. Sorace and R. Sessoli, *J. Am. Chem. Soc.*, **2017**, *139*, 4338-4341.
[51] R. Boča, C. Rajnák, J. Titiš and D. Valigura, *Inorg. Chem.*, **2017**, *56*, 1478-1482.
[52] W. Lin, T. Bodenstein, V. Mereacre, K. Fink and A. Eichhöfer, *Inorg. Chem.*, **2016**, *55*, 2091-2100.
[53] L. Tesi, E. Lucaccini, I. Cimatti, M. Perfetti, M. Mannini, M. Atzori, E. Morra, M. Chiesa, A. Caneschi, L. Sorace and R. Sessoli, *Chem. Sci.*, **2016**, *7*, 2074-2083.
[54] L. Tesi, A. Lunghi, M. Atzori, E. Lucaccini, L. Sorace, F. Totti and R. Sessoli, *Dalton Trans.*, **2016**, *45*, 16635-16643.
[55] S.-Q. Wu, Y. Miyazaki, M. Nakano, S.-Q. Su, Z.-S. Yao, H.-Z. Kou and O. Sato, *Chem. Eur. J.*, **2017**, *23*, 10028-10033.